Phases of active matter composed of multicellular magnetotactic bacteria near a hard surface

Alexander Petroff,[1] Alejandra Rosselli-Calderon,[1] Ben Roque,[1] and Pradeep Kumar[2]
[1]*Department of Physics, Clark University, Worcester, Massachusetts 01610, USA*
[2]*Department of Physics, University of Arkansas, Fayetteville, Arizona 72701, USA*

(Received 8 June 2021; accepted 20 April 2022; published 27 May 2022)

We investigate the motion of *multicellular magnetotactic bacteria* (MMB) near a hard surface. Directing MMB towards a flat surface causes them to accumulate about the wall as an active gas. MMB are exponentially distributed about the surface with a penetration depth determined by the typical distance an MMB swims before it aligns with the ambient field. Increasing the magnetic field past a critical value, at which the penetration depth is of order the size of an MMB, causes the active gas to condense into a two-dimensional active fluid. Measurements of MMB motion in this phase reveal that contact with the surface enhances rotational diffusion by a factor of 8 and that velocity fluctuations are Laplace distributed. The fluid undergoes a percolation transition at a critical magnetic field. Supercritical active fluids exhibit dynamic voids, which limit the relaxation of density fluctuations. We describe the possible ecological significance of these results.

DOI: 10.1103/PhysRevFluids.7.053102

I. INTRODUCTION

Understanding the strategies by which microbes navigate complex environments gives insight into their ecology and evolution and provides inspiration for engineers [1–4]. A variety of microbes living in sediment have independently evolved [5] the ability to navigate the labyrinthine pore spaces in which they live using the geomagnetic field [6]. Because, at high latitudes, Earth's magnetic field has a substantial radial component, swimming along magnetic field lines allows cells to position themselves in the continuously changing vertical chemical gradients typical of natural sediment [5]. However, if cells exclusively swim along field lines they are quickly trapped when they inevitably collide with an obstacle (e.g., a grain of sand). The strategies that allow magnetotactic cells to balance motion along field lines with obstacle avoidance remain poorly understood. To elucidate the physical basis of these strategies, we investigate the motion of one type of magnetotactic bacteria near a hard surface [7].

We focus on a group of δ proteobacteria commonly called *multicellular magnetotactic bacteria* (MMB), which have been assigned the provisional name *Candidatus* Magnetoglobus multicellularis [8]. These cells are the only known obligately multicellular bacteria [9]. These cells exclusively live in spherical colonies (see Fig. 1) composed of a monolayer of $\sim$50 bacteria [10,11]. Ninety-five percent of colonies have diameters between 3.8 and 7.3 μm with a mean diameter of 5.3 μm. Fewer that 1% of colonies, which are close to dividing [Fig. 1(e)], can reach diameters of 10.8 μm. Cells in an MMB colony cooperate to push the colony along magnetic field lines with a typical speed of $U = 75$ μm/s. Each cell in an MMB colony precipitates magnetic crystals, either magnetite [12] or greigite [13], which cause the colony to align its average magnetic moment with the ambient magnetic field. The outer surface of each cell is covered with about 30 flagella [14,15]. The constituent cells exert an average force that is parallel to within a few degrees of the net magnetic

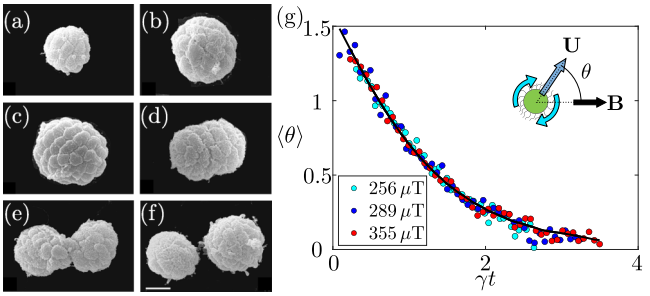

FIG. 1. Multicellular magnetotactic bacteria live in spherical colonies composed of about 50 bacteria that grow and move like a single organism [22]. (a)–(f) As the cells in a colony divide, the colony grows, elongates, and divides symmetrically. The scale bar is 4 μm. Panels (a)–(f) are modified slightly from Ref. [11] for legibility. Panel (g) shows the angle θ between the colony velocity $\mathbf{U}$ and the ambient magnetic field $\mathbf{B}$ averaged over several hundred colonies as they turn to align with the field. The average alignment rate γ is fit for each magnetic field. The solid black line is the solution of Eq. (1).

moment [16]. The colonies swim through the fluid without tumbling, though a few colonies rarely ($\approx 1/60$ s^{-1}) reverse their motion to briefly swim against the imposed magnetic field [17].

Two torques guide an MMB colony through the confined geometry of the pore space. The magnetic torque on a colony causes it to align with the ambient magnetic field B at a rate of $\gamma = mB/8\pi\mu a^3$, where m is the magnetic moment, μ is the viscosity of water, and a is the colony radius. MMB, moving with speed U, swim a typical distance of $\ell = 8\pi\mu a^3 U/mB$ as they align with the magnetic field. When a colony approaches within a distance $\sim a$ of a surface, hydrodynamic interactions with the surface can turn the colony [18–20].

We tune the ratio of the length scales ℓ/a over which these two processes act by varying B. At low magnetic fields, for which $\ell/a \sim 30$, colonies quickly escape into the bulk fluid, where the magnetic field turn them back towards the surface. This process of collision and alignment causes colonies to accumulate near a surface like an active gas. Increasing the magnetic field such that $\ell/a \sim 1$ causes this active gas to condense on the surface as an active two-dimensional fluid. Examining the dynamics of this active fluid reveals that contact with a surface increases the rotational diffusion coefficient by a factor of 8.

II. RESULTS

A. Enrichment of MMB

MMB have not been grown in pure culture. We enrich them from sediment taken from a shallow pool in a Massachusetts salt marsh (41°34′34.2″ N, 70°38′21.4″ W) between late spring and early fall and maintained in the laboratory. We lightly stir the sediment and place a neodymium magnet near the sediment surface [14,21]. After 20 min, we collect 1 ml of water near the magnet surface. This material is placed in a vial, mixed lightly, and placed next to a magnet for an additional 20 min. By collecting the 0.1 ml of water near the magnet surface, we find thousands of MMB colonies, which represent the overwhelming majority of cells.

B. MMB motion in the bulk fluid

We begin by characterizing the motion of free-swimming MMB in an applied magnetic field [17]. We inoculate MMB colonies into a rectangular microfluidic chamber (1.5 cm×1 cm×0.015 cm), composed primarily of polydimethylsiloxane and sealed on one side with a glass slide. We focus a microscope (Olympus X71, 20× objective) on a plane halfway between the top and the bottom of the chamber. The entire experiment is performed inside a three-axis Helmholtz coil (Walker

Scientific, 76-cm coils), which creates a magnetic field **B** as large as 600 μT with 1-μT precision; the magnetic field varies over the field of view by less than 0.03%.

We initially apply a constant magnetic field of 256 μT and measure the angle $\theta(t)$ between the velocity **U** of each colony and **B** at time t. MMB swim with an average speed of $U = 75$ μm/s, although individual colonies show substantial variability in the range of 45 to 134 μm/s (95% confidence interval). Although their average direction of motion is parallel to the applied field, rotational diffusion causes their direction to slightly fluctuate with $\langle\theta^2\rangle = 0.17$ rad^2. By switching the magnetic coils through which current flows, we rotate the field by 90° and measure $\theta(t)$ as MMB align with the new field (see Fig. 1(g), Supplemental Video SV1, and Supplemental Fig. S1 [23]).

To measure the magnetic moment m and the rotational diffusion coefficient D_r of MMB colonies, we compare these trajectories to the two-dimensional motion of a colony that swims at a constant speed parallel to its magnetic moment, which passively rotates to align with the ambient field [24,25]. Combining this deterministic motion with rotational Brownian motion gives the angular velocity

$$\frac{d\theta}{dt} = -\gamma \sin(\theta) + \sqrt{2D_r}\eta(t), \tag{1}$$

where η is white noise with $\langle\eta(t)\rangle = 0$ and $\langle\eta(t)\eta(t')\rangle = \delta(t - t')$. The colony swims with velocity

$$\mathbf{U} = U[\cos(\theta)\hat{x} + \sin(\theta)\hat{y}], \tag{2}$$

where $\hat{x}$ and $\hat{y}$ are unit vectors parallel and perpendicular to the applied field, respectively. As shown in Fig. 1(g), the measured trajectories of swimming MMB colonies are in good agreement with this model. At 256 μT, we find $\gamma = 1.24 \pm 0.02$ s^{-1}. The rotational diffusion coefficient $D_r = \langle\theta^2\rangle\gamma = 0.212 \pm 0.003$ rad^2/s is measured from the trajectories before the field was rotated. Its value is roughly similar to that of the eukaryotic alga *Chlamydomonas reinhardtii* (0.4 rad^2/s) [18]. By fitting the trajectories of 128 individual MMB colonies, we find the natural variability of magnetic moments in the sample to range from 3.9×10^{-15} to 10.9×10^{-15} Am^2 (95% confidence interval) [26].

C. An active gas of MMB near a surface

Next, we investigate how the motion of MMB changes as they are scattered from a surface. We apply a field to direct MMB to collide normal to the chamber wall. We begin by considering a null model of colony-surface interference. If the surface principally acts to cancel the normal component of the colony velocity, the rate k_e at which MMB escape is the rate at which rotational diffusion turns the colony away from the surface. Given a correlation time γ^{-1} of fluctuations, $k_e \approx \gamma\,\mathrm{erf_c}(\sqrt{\pi^2\gamma/8D_r})$. At a magnetic field of 0.29 mT, the expected rate of escape is $k_e = 7\times10^{-5}$ s^{-1}. We therefore expect that, once a colony collides with a surface, it will remain trapped for several hours.

In contrast to this naïve estimate, when a colony collides with the chamber wall, it is only in contact for a fraction of a second before it escapes back into the bulk fluid (Fig. 2(a) and Supplemental Video SV2 [23]), where it realigns with the ambient field. The measured concentration n of colonies, normalized by the concentration at the surface n_0, at a distance X from the wall [Fig. 2(b)] is consistent with an exponential decay. As we increase the magnitude of the magnetic field, the exponential profiles become more sharp as colonies are confined more closely to the wall. The penetration depth λ of colonies into the bulk fluid is proportional to the turning length ℓ; we find $\lambda/\ell = 1.5 \pm 0.04$. We conclude that colonies scatter after a collision with a surface into the bulk fluid, where they realign with the ambient field and collide with the surface again.

D. Formation of a two-dimensional active fluid

These results imply that at a critical magnetic field $B = 8\pi\mu a^2/m \sim 4$ mT, the turning radius ℓ shrinks to the size of a single MMB colony. At such a high magnetic field, we expect the active gas

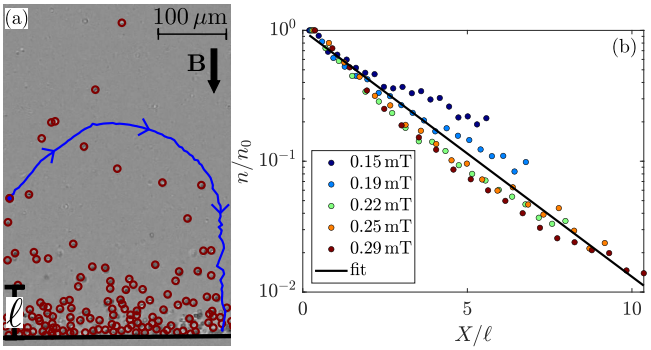

FIG. 2. MMB scatter from a surface. (a) A snapshot of an experiment ($B = 0.29\,\mathrm{mT}$) is shown. Red circles show positions of colonies near the chamber wall (black line). The blue curve shows the trajectory of a colony that collided with the wall. (b) Colonies are distributed exponentially about the wall. The distance X from the wall is normalized by ℓ. The black line shows the best-fit exponential.

of free-swimming MMB colonies to condense on the surface as a two-dimensional phase of active matter.

We modify our experiments to visualize this state of active matter [see Fig. 3(a)]. To generate the relatively high magnetic fields required, we wrap a 40× microscope objective with 1000 turns of copper wire. We generate fields between 0.9 and 4.0 mT measured at the focal distance of the objective. We inoculate a chamber composed of a glass slide and a coverslip separated by a 250-μm plastic spacer (Gene Frame, ThermoFisher Scientific, USA). We focus the microscope to just below the height of the coverslip.

As we increase the magnetic field, we observe the emergence of a two-dimensional fluid phase [25,27]. At high magnetic field ($B > 2.0\,\mathrm{mT}$), MMB colonies display roughly hexagonal order [28–31] (see Figs. 3(b) and 6 and see Supplemental Video SV3 [23]) with many vacancies. We measure the concentration of colonies and extract their positions, velocities, and trajectories over the course of 1 min. The concentration of colonies on the surface increases linearly with B to an area fraction of 0.61 at $B = 3.2\,\mathrm{mT}$, where it saturates. Removing the magnetic field causes colonies to rapidly escape to the bulk fluid, implying that the magnetic field produced by the MMB is insufficient to trap colonies [25].

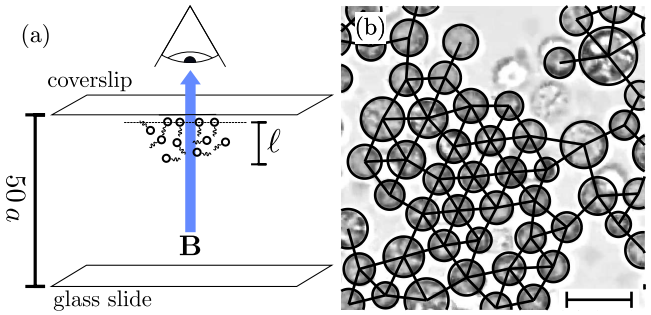

FIG. 3. MMB are directed to collide normal to a coverslip by an applied magnetic field. (a) A schematic of the experiment is shown. The microscope is focused one colony radius below the top surface. (b) At the highest magnetic field examined (4 mT), colonies localize on the glass surface, where they diffuse laterally and collide with one another. The contact network is shown to highlight the local hexagonal order of the active fluid and the many vacancies, dislocations, and voids. The scale bar is 10 μm.

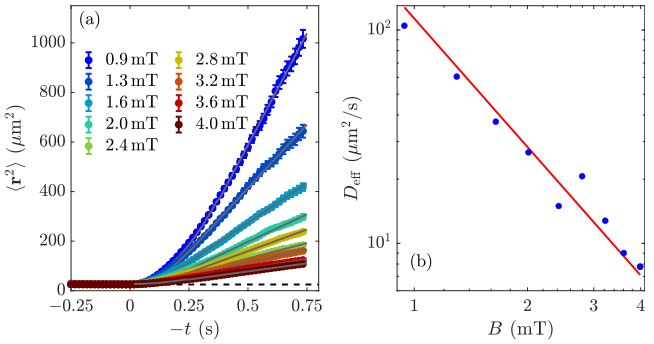

FIG. 4. At high magnetic field, MMB diffuse laterally over the chamber wall. (a) The measured distance $\mathbf{r}$ between isolated colonies at a time $-t$ before they collide is consistent with the motion of hard Brownian disks; we fit the two-dimensional diffusion coefficient $D_{\rm eff}$ at each magnetic field. The solid line is quadratic for $-t < \tau_{\rm B}$ and then increases linearly with slope $16D_{\rm eff}$ [32]. (b) $D_{\rm eff}$ decreases with increasing magnetic field. The red line shows the fit to $D_{\rm eff} = \alpha B^{-2}$.

E. Dynamics of individual MMB in an active fluid

We begin our analysis by studying the motion of isolated colonies as they move over the two-dimensional glass surface. A colony may move laterally over the surface either because it exerts a force or it is advected by the flows generated by a nearby colony [29]. To disentangle these two components of motion we examine the trajectories of isolated colonies shortly before they collide. We find [Fig. 4(a)] that the the root-mean-squared distance $\langle r^2 \rangle$ initially grows quadratically with time, consistent with ballistic motion, up to a time τ_B, after which $\langle r^2 \rangle$ grows linearly in time. The timescale for ballistic motion τ_B increases in proportion to γ^{-1}, indicating that colonies tumble for as long as their magnetic moment is misaligned from the ambient field. We conclude that the colonies move over the surface like noninteracting hard Brownian disks and that the influence of advection by neighboring colonies is imperceptible.

Fitting the effective two-dimensional diffusion coefficient $D_{\rm eff}$ to these trajectories [32], we find reasonably large values of $D_{\rm eff}$ [Fig. 4(b)], which decrease with the applied magnetic field. At the lowest magnetic field, $D_{\rm eff} = 104 \pm 3\ \mu\text{m}^2/\text{s}$.

Next, we use these measurements to infer the rotational diffusion coefficient of colonies near the surface. The in-plane diffusion coefficient $D_{\rm eff} = \langle v_t^2 \rangle / 2\gamma$ [33], where v_t is the speed tangential to the chamber wall. From Eq. (2), colonies move laterally with velocity $v_t = U \sin(\theta)$. At high magnetic field, $\langle v_t^2 \rangle \approx U^2 \langle \theta^2 \rangle = U^2 D_r / \gamma$. Note that increasing the magnetic field decreases both the timescale for ballistic motion and the typical speed (see Supplemental Material [23], Fig. S3). Combining these effects, $D_{\rm eff} = U^2 D_r / 2\gamma^2$. Fitting the measured diffusion coefficients at various magnetic fields to this model [Fig. 4(b)], we find $D_r = 1.6\ \text{rad}^2/\text{s}$. We conclude that the rotational diffusion coefficient of colonies near a surface is eight times greater than that of free-swimming colonies ($D_r = 0.212\ \text{rad}^2/\text{s}$).

To understand how the increase in rotational diffusion is reflected in the motion of colonies, we measure the distribution of instantaneous velocities v_t for all the colonies in the field of view, including those in contact with others. At the lowest magnetic field examined, v_t is Laplace distributed (Fig. 5), in stark contrast to the Gaussian fluctuations predicted by Eq. (1) and observed in the motion of free-swimming colonies (see Supplemental Material [23], Fig. S2). As the magnetic field increases, the distribution becomes Gaussian for small v_t, but the exponential tails remain.

This anomalous behavior can be understood as a consequence of the multicellular nature of the colonies. Equations (1) and (2) implicitly assume that the coordinated action of the cells in a colony can be approximated as a single point force. In reality, each cell exerts a force on the colony. Consider the effect of a single cell on the motion of the colony. By Eq. (1), an individual cell

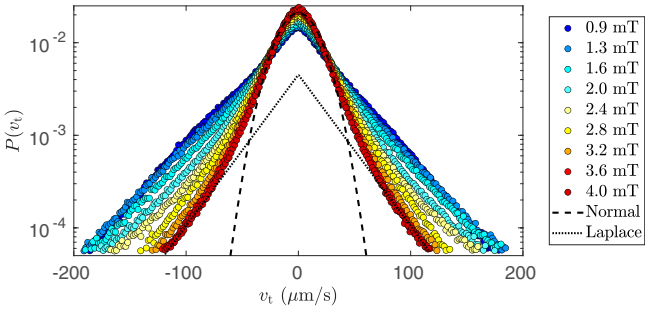

FIG. 5. The probability density functions of tangential velocities of colonies are shown for a range of magnetic fields. The number of instantaneous measurements from which the distributions is calculated range from 6.5×10^5 ($B = 0.9$ mT) to 1.6×10^6 ($B = 4.0$ mT). Normal and Laplace distributions are shown as guides to the eye.

produces velocity fluctuations that are normally distributed $\mathcal{N}(v_t, w)$ with zero mean and variance w. As the component of the force exerted by different cells tangential to the wall varies with the position of the cell in the colony, the motion of the colony is a weighted sum over the forces exerted by each cell. Approximating the sum over the several tens of cells in a colony as an integral and assuming an exponential distribution $p(w) = e^{-w/2b^2}/2b^2$ of weights [34], the weighted sum

$$P(v_t) = \int_0^\infty \mathcal{N}(v_t, w)p(w)dw = \frac{1}{2b}e^{-|v_t|/b} \tag{3}$$

is Laplace distributed.

While this analysis is promising, a model is needed to explain why the weighting function $p(w)$ would be exponentially distributed. We speculate that collisions between the hundreds of flagella covering the colony and the surface could be dynamically important in reorienting the colony. The length of the flagella and the diameter of the colony may set the scale of the exponential decay.

F. Dynamics of the active fluid

We now provide a brief overview of the large-scale dynamics of the active fluid, which will be the focus of a future paper. As shown in Fig. 6(e), active fluids undergo a percolation transition [35]. This transition arises as the concentration of MMB trapped on the surface increases with the applied magnetic field. From each frame of the recorded videos, we extract the center of each colony and reconstruct the contact network. To account for the polydisperse size distribution of colonies, we infer contacts between colonies that are separated by less than twice the average colony diameter. We measure the distribution in the number N of colonies in connected clusters. The variance in cluster size—averaged over the 1-min experiment—increases sharply and exhibits a maximum at the critical magnetic field $B_c \approx 2.0$ mT [Fig. 6(e)]. At this magnetic field a spanning cluster emerges. The weight P_s of the spanning cluster increases with the magnetic field. The packing fraction 0.46 of colonies at the critical magnetic field is substantially less than the value predicted [36] for hard disks (0.673), suggesting slight adhesion [37] or motility-induced phase separation [38] cause colonies to cluster.

We measure the pair-correlation function and the structure factor of the active fluids at each magnetic field [39,40]. The pair-correlation function $g(r)$ is consistent with that of a fluid; as the magnetic field increases $g(r)$ develops secondary and tertiary peaks [see Fig. 6(f)], which suggests that the active fluid becomes more structured with the increase in the magnetic field. Moreover, we find that the structure factor $S(q) = \langle\rho(q)\rho(-q)\rangle/N$—where $\rho(q)$ is the Fourier transform of the density and N is the number of colonies—is sharply peaked at low wave number q [see Fig. 6(g)], indicating that the fluid is compressible.

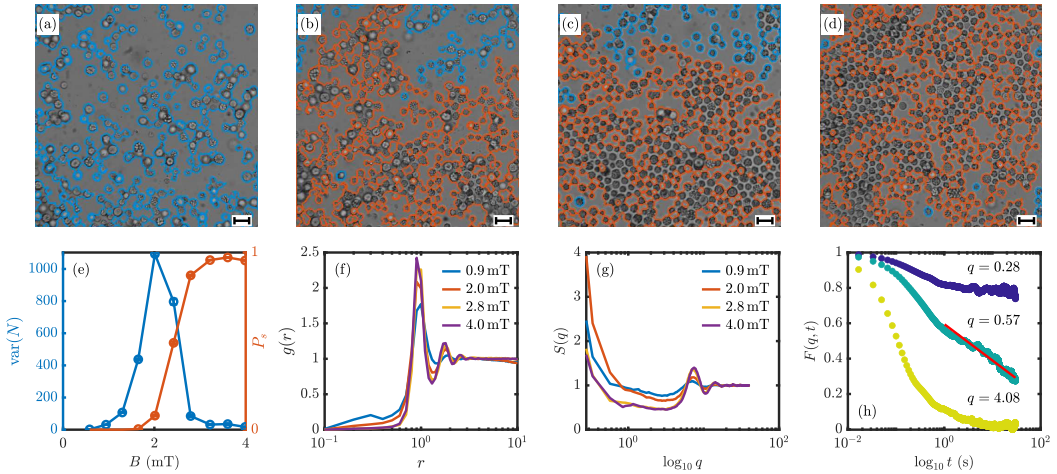

FIG. 6. Colonies self-organize into active fluids. Increasing the magnetic field increases the concentration of colonies but decreases their effective temperature. Representative snapshots show the geometry of the active fluids at magnetic fields (a) 0.9 mT, (b) 2.0 mT, (c) 2.8 mT, and (d) 4.0 mT. Blue curves and red curves show the boundaries of finite clusters and spanning clusters, respectively. Scale bars are 10 μm. (e) The fluids undergo a percolation transition at a critical magnetic field $B_c \approx 2$ mT. Near B_c, the spanning cluster rapidly appears and disappears as colonies reorganize. The distribution of cluster sizes N and the weight of the spanning cluster are averaged in time. The pair-correlation function $g(r)$ [panel (f)] and the structure factor $S(q)$ [panel (g)] are consistent with a compressible fluid. (h) The intermediate scattering function is shown for $B = 4.0$ mT. All distances r and wave numbers q are measured relative to the average colony diameter.

The most striking feature of the active fluids at the highest magnetic field is the persistence of large voids [Fig. 6(d) and Supplemental video SV3 [23]). Voids form continuously as colonies escape from the glass surface. These voids diffuse through the active fluid, coarsen as they merge, and diminish as escaped colonies collide with the coverslip. The average area of voids evolves as a random walk. The instantaneous changes in void areas are—like the velocity of individual colonies—Laplace distributed (see Fig. 7). A time series of the average void area shows a $1/f$ spectrum.

To characterize the effect of voids on the dynamics of the active fluid at the highest magnetic field, we measure the intermediate scattering function [39]

$$F(q,t) = \frac{\langle \rho(q,t)\rho(-q,0)\rangle}{\langle \rho(q,0)^2\rangle}. \tag{4}$$

Figure 6(h) shows $F(q,t)$ for three values of q at the highest magnetic field. On scales similar to the size of a colony ($2\pi/q = 1.5$ colony diameters), density fluctuations decay diffusively. The relaxation of density fluctuations on the scale of $2\pi/q = 23$ colony diameters reaches a plateau over the timescale of our measurements, and the system is presumably arrested either by a jamming transition (area fraction $\phi = 0.6$) or possibly very slow glassy relaxation. At intermediate length scales ($2\pi/q = 11$ colony diameters) similar to the size of voids, the density fluctuations appear to relax logarithmically. A similar logarithmic decay is observed for Brownian particles diffusing in an evolving pore space [41]. This similarity suggests that relaxation is limited by the time it takes large voids to form, through which colonies can diffuse. In future work, we plan to extend the timescale of the experiment to see if the slow relaxation is truly logarithmic or if it is an intermediate state in a two-step decay.

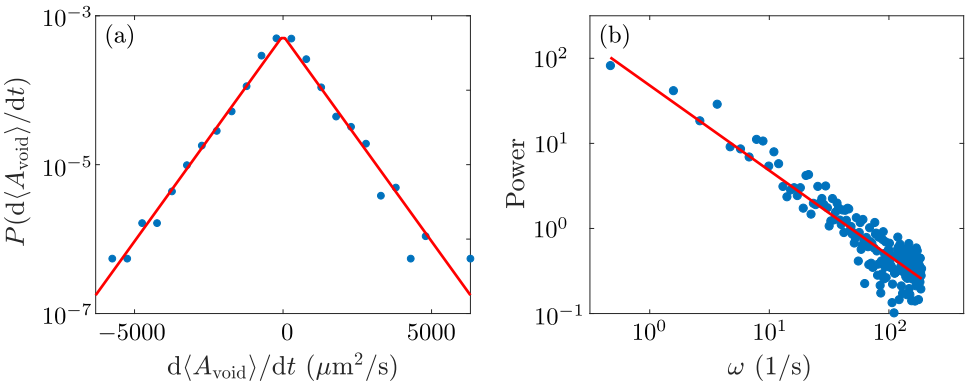

FIG. 7. The two-dimensional active fluid formed by colonies at the highest magnetic field examined (4 mT) shows a prevalence of large voids. The typical size of a void $\approx 200\ \mu\mathrm{m}^2$ is much larger than the cross-sectional area of a colony $40\ \mu\mathrm{m}^2$. Voids form as colonies escape the surface. The voids diffuse through the fluid and merge (see Supplemental Video SV3.avi [23]). To characterize these dynamics we measure the average area $\langle A_{\mathrm{void}}\rangle$ of voids that are entirely surrounded by colonies. (a) Like the velocity fluctuations of individual colonies, instantaneous fluctuations of void areas are Laplace distributed. The average change is zero, consistent with the persistence of voids. (b) The power spectrum of the time series shown in panel (a) shows a $1/f$ dependence (red curve).

III. DISCUSSION AND CONCLUSION

We have experimentally investigated the motion of MMB near a surface. At relatively low magnetic fields, MMB accumulate within a typical distance ℓ from a surface like an active gas. At a critical magnetic field, at which the typical distance ℓ a colony swims into the bulk fluid decreases to the diameter of a colony, the active gas condenses into an active two-dimensional fluid. Tracking individual colonies in the active fluid reveals that the rotational diffusion coefficient of the colonies increases by a factor of 8 when they are in contact with a surface and velocity fluctuations are Laplace distributed rather than normally distributed. As the applied magnetic field increases, the concentration of colonies in the active fluid increases, which leads to a percolation transition. Density fluctuations on the scale of the void space of the fluid appear to relax logarithmically in time.

We turn now to the possible ecological and evolutionary significance of these results. In the natural environment, where the ambient geomagnetic field is $B_{\mathrm{geo}} = 51.9\ \mu\mathrm{T}$, the turning radius of the colony $\ell \approx 300\ \mu\mathrm{m} \gg a$. Consequently, colonies accumulate about obstructions as an active gas. This random motion could facilitate navigation through the labyrinthine pore space. MMB use the the geomagnetic field to navigate the vertical chemical gradients in the top millimeters of sediment [5]. To successfully navigate through the pose space, MMB must balance motion along field lines with motion around obstacles. We define the scattering number $\mathrm{Sc} = \gamma/k_{\mathrm{sc}}$ as the ratio of the rate γ at which MMB align with the magnetic field to the rate k_{sc} at which colonies orient their motion in random directions. If $\mathrm{Sc} \gg 1$, colonies move deterministically along field lines. Such colonies are unable to navigate the complex pore space because they become trapped as soon as they collide with a surface. If $\mathrm{Sc} \ll 1$, colonies move diffusively through the sediment and cannot align with the ambient field. Thus, natural selection may tune the phenotype of colonies such that $\mathrm{Sc} \sim 1$. Having found that MMB scatter upon collision with a surface, we estimate the scattering rate from the time U/ℓ_p required for an MMB to swim one pore diameter $\ell_p \approx 0.1$ mm. Indeed, in the local geomagnetic field B_{geo}, $\mathrm{Sc} = mB_{\mathrm{geo}}U/8\pi\mu a^3\ell_p \approx 1/3$. This scaling can be rewritten to highlight the reflection of environment on the phenotype as

$$\frac{mU}{a^3} \sim \frac{8\pi\mu\ell_p}{B_{\mathrm{geo}}}, \tag{5}$$

where the left-hand side describes the phenotype of the colony, upon which natural selection can act, and the right-hand side is determined by the environment.

ACKNOWLEDGMENTS

We would like to thank A. Libchaber, C. Modes, A. Kudrolli, H. Gould, and O. Devauchelle for their comments. We are grateful to J. Norton, M. Hanout, and C. Mitchell for their assistance. R. Hatzenpichler provided invaluable suggestions for the enrichment of MMB. This work was supported by the American Chemical Society (Grant No. ACS PRF 60426-DNI2) and partially by the National Science Foundation (Grant No. NSF PHY-2042150). Bruce Weiller provided additional funding for A.R.-C.

APPENDIX

Tracking the motion of swimming colonies allows us to measure their magnetic moments and rotational diffusion coefficients and characterize the dynamics of active fluids. We track colonies in two experiments. In the first experiment, colonies swim in a microfluidic chamber. The applied magnetic field is orthogonal to the optical path used to visualize the colonies. In the second experiment, colonies are directed towards a coverslip. The optical path is parallel to the magnetic field. These differences require different approaches to identify the positions of colonies in each frame.

Colonies swimming in the microfluidic device appear as dark circles on a bright background (see Supplemental Videos SV1.avi and SV2.avi [23]). The large contrast difference between free-swimming colonies and the background makes tracking the colonies relatively simple. We first average all the frames from the video to find the background light intensity. Subtracting the background intensity from each frame highlights the positions of the colonies. We then apply an intensity threshold and extract the centroid of each dark disk. The trajectories of the centroids are extracted using the MATLAB function "assignDetectionsToTracks."

In the second experiment, colonies move laterally over the chamber surface. In these experiments, the scattering of light through the individual cells that compose the colonies gives each colony a textured appearance when it is in focus (see Supplemental Video SV3.avi [23]). Colonies swimming below the focal plane appear as bright disks with dark halos. The textured appearance of colonies and their close proximity to each other make the extraction of their positions challenging. We identify the position of colonies in three steps. We first average all of the frames in the video to find the background illumination, which we subtract from each frame. Next, to highlight the texture of each colony, we measure the local standard deviation of the image; at each point in the frame we measure the standard deviation of pixel intensities in a neighborhood of one half of a colony radius. Finally, we identify circular components in the image of the local standard deviation by using the MATLAB function "imfindcircles," which computes the circular Hough transform. We adjust the parameters in this procedure to eliminate false positives. Comparing the positions of colonies identified by this method to the original images, we find a rate of about 15% of false negatives and very few false positives. We use these instantaneous measurements of positions to calculate the contact network, the pair-correlation function, the scattering function, and the intermediate scattering function (see main text, Fig. 6). We extract the trajectories of colonies from their positions using the MATLAB function "assignDetectionsToTracks." Doing so allows us to calculate their instantaneous velocities and measure the distance between isolated colonies immediately before a collision (see main text, Figs. 4 and 5).

To test the sensitivity of these results to the considerable number of false negatives, we developed a complementary method to identify connected clusters of colonies. Again, we begin by subtracting the background image from each frame to remove inhomogeneities in illumination. Next, we apply an intensity threshold to identify regions of the image that are occupied by colonies. While the colonies are textured, the average intensity is darker than the background. The resulting binary

image includes all of the colonies in the image as well as the dark halos of colonies swimming below the focal plane. Next, we find the connected components formed by colonies in contact with each other. To do so, we first dilate the binary image using a circular neighborhood of three pixels (about one-tenth the colony radius). After dilating the image three times, we then erode the binary image three times using the same circular filter. This process of dilation and erosion fills in small holes and connects colonies that are close together. The perimeters of these clusters are shown in Fig. 6 and Supplemental Video SV3 [23]. Computing the weight of the spanning cluster and the variance of cluster areas shows the same percolation transition at a critical magnetic field of 2 mT as found from the reconstructed contact network.

[1] T. Fenchel, Microbial behavior in a heterogeneous world, Science **296**, 1068 (2002).

[2] H. H. Wensink, V. Kantsler, R. E. Goldstein, and J. Dunkel, Controlling active self-assembly through broken particle-shape symmetry, Phys. Rev. E **89**, 010302(R) (2014).

[3] H. Wioland, F. G Woodhouse, J. Dunkel, and R. E. Goldstein, Ferromagnetic and antiferromagnetic order in bacterial vortex lattices, Nat. Phys. **12**, 341 (2016).

[4] J. Cammann, F. J. Schwarzendahl, T. Ostapenko, D. Lavrentovich, O. Bäumchen, and M. G. Mazza, Emergent probability fluxes in confined microbial navigation, Proc. Natl. Acad. Sci. USA **118**, e2024752118 (2021).

[5] R. P. Blakemore, Magnetotactic bacteria, Annu. Rev. Microbiol. **36**, 217 (1982).

[6] N. Waisbord, A. Dehkharghani, and J. S. Guasto, Fluidic bacterial diodes rectify magnetotactic cell motility in porous environments, Nat. Commun. **12**, 5949 (2021).

[7] C. N. Keim, D. M. da Silva, R. D. de Melo, D. Acosta-Avalos, M. Farina, and H. L. de Barros, Swimming behavior of the multicellular magnetotactic prokaryote 'Candidatus Magnetoglobus multicellularis' near solid boundaries and natural magnetic grains, Antonie van Leeuwenhoek **114**, 1899 (2021).

[8] F. Abreu, J. L. Martins, T. S. Silveira, C. N. Keim, H. G. P. L. de Barros, F. J. Gueiros Filho, and U. Lins, '*Candidatus* Magnetoglobus multicellularis', a multicellular, magnetotactic prokaryote from a hypersaline environment, Int. J. Syst. Evol. Microbiol. **57**, 1318 (2007).

[9] N. A. Lyons and R. Kolter, On the evolution of bacterial multicellularity, Curr. Opin. Microbiol. **24**, 21 (2015).

[10] C. T. Lefèvre and D. A. Bazylinski, Ecology, diversity, and evolution of magnetotactic bacteria, Microbiol. Mol. Biol. Rev. **77**, 497 (2013).

[11] C. N. Keim, J. L. Martins, F. Abreu, A. S. Rosado, H. L. de Barros, R. Borojevic, U. Lins, and M. Farina, Multicellular life cycle of magnetotactic prokaryotes, FEMS Microbiol. Lett. **240**, 203 (2004).

[12] U. Lins, C. N. Keim, F. F. Evans, M. Farina, and P. R. Buseck, Magnetite (Fe_3O_4) and greigite (Fe_3S_4) crystals in multicellular magnetotactic prokaryotes, Geomicrobiol. J. **24**, 43 (2007).

[13] F. Abreu, K. T. Silva, M. Farina, C. N. Keim, and U. Lins, Greigite magnetosome membrane ultrastructure in 'Candidatus Magnetoglobus multicellularis', Int. Microbiol. **11**, 75 (2008).

[14] F. G. Rodgers, R. P. Blakemore, N. A. Blakemore, R. B. Frankel, D. A. Bazylinski, D. Maratea, and C. Rodgers, Intercellular structure in a many-celled magnetotactic prokaryote, Arch. Microbiol. **154**, 18 (1990).

[15] K. T. Silva, F. Abreu, F. P. Almeida, C. N. Keim, M. Farina, and U. Lins, Flagellar apparatus of south-seeking many-celled magnetotactic prokaryotes, Microsc. Res. Tech. **70**, 10 (2007).

[16] F. P. Almeida, N. B. Viana, U. Lins, M. Farina, and C. N. Keim, Swimming behaviour of the multicellular magnetotactic prokaryote 'Candidatus magnetoglobus multicellularis' under applied magnetic fields and ultraviolet light, Antonie van Leeuwenhoek **103**, 845 (2013).

[17] M. Greenberg, K. Canter, I. Mahler, and A. Tornheim, Observation of magnetoreceptive behavior in a multicellular magnetotactic prokaryote in higher than geomagnetic fields, Biophys. J. **88**, 1496 (2005).

[18] K. Drescher, J. Dunkel, L. H. Cisneros, S. Ganguly, and R. E. Goldstein, Fluid dynamics and noise in bacterial cell–cell and cell–surface scattering, Proc. Natl. Acad. Sci. USA **108**, 10940 (2011).

[19] E. Lauga and T. R. Powers, The hydrodynamics of swimming microorganisms, Rep. Prog. Phys. **72**, 096601 (2009).
[20] E. Lushi, V. Kantsler, and R. E. Goldstein, Scattering of biflagellate microswimmers from surfaces, Phys. Rev. E **96**, 023102 (2017).
[21] O. H. Shapiro, R. Hatzenpichler, D. H. Buckley, S. H. Zinder, and V. J. Orphan, Multicellular photomagnetotactic bacteria, Environ. Microbiol. Rep. **3**, 233 (2011).
[22] C. N. Keim, M. Farina, and U. Lins, Magnetoglobus, magnetic aggregates in anaerobic environments, Microbe–Am. Soc. Microbiol. **2**, 437 (2007).
[23] See Supplemental Material at http://link.aps.org/supplemental/10.1103/PhysRevFluids.7.053102 for three videos and three additional figures. Video SV1: MMB colonies turn in a rotated magnetic field. Video SV2: MMB colonies collide with and escape from a hard surface at three magnetic fields. Video SV3: Colonies self-organize into active fluids. Figure S1: Trajectories of colonies as they align with an imposed magnetic field. Figure S2: The orientations of a free-swimming colony about an imposed magnetic field are normally distributed. Figure S3: Instantaneous velocity fluctuations of colonies in an active decrease inversely with the magnitude of the applied magnetic field.
[24] A. Kalmijn, Biophysics of geomagnetic field detection, IEEE Trans. Magn. **17**, 1113 (1981).
[25] C. J. Pierce, H. Wijesinghe, E. Mumper, B. H. Lower, S. K. Lower, and R. Sooryakumar, Hydrodynamic Interactions, Hidden Order, and Emergent Collective Behavior in an Active Bacterial Suspension, Phys. Rev. Lett. **121**, 188001 (2018).
[26] M. Perantoni, D. M. S. Esquivel, E. Wajnberg, D. Acosta-Avalos, G. Cernicchiaro, and H. L. de Barros, Magnetic properties of the microorganism Candidatus Magnetoglobus multicellularis, Naturwissenschaften **96**, 685 (2009).
[27] X.-L. Wu and A. Libchaber, Particle Diffusion in a Quasi-Two-Dimensional Bacterial Bath, Phys. Rev. Lett. **84**, 3017 (2000).
[28] I. H. Riedel, K. Kruse, and J. Howard, A self-organized vortex array of hydrodynamically entrained sperm cells, Science **309**, 300 (2005).
[29] A. P. Petroff, X.-L. Wu, and A. Libchaber, Fast-Moving Bacteria Self-Organize into Active Two-Dimensional Crystals of Rotating Cells, Phys. Rev. Lett. **114**, 158102 (2015).
[30] J. Palacci, S. Sacanna, A. P. Steinberg, D. J. Pine, and P. M. Chaikin, Living crystals of light-activated colloidal surfers, Science **339**, 936 (2013).
[31] T. H. Tan, A. Mietke, H. Higinbotham, J. Li, Y. Chen, P. J. Foster, S. Gokhale, J. Dunkel, and N. Fakhri, Development drives dynamics of living chiral crystals, arXiv:2105.07507.
[32] A. P. Petroff and A. Libchaber, Nucleation of rotating crystals by *Thiovulum majus* bacteria, New J. Phys. **20**, 015007 (2018).
[33] H. C. Berg, *Random Walks in Biology* (Princeton University Press, Princeton, NJ, 2018).
[34] B. Wang, J. Kuo, S. C. Bae, and S. Granick, When Brownian diffusion is not Gaussian, Nat. Mater. **11**, 481 (2012).
[35] D. Stauffer and A. Aharony, *Introduction to Percolation Theory* (Taylor & Francis, London, 2018).
[36] S. Mertens and C. Moore, Continuum percolation thresholds in two dimensions, Phys. Rev. E **86**, 061109 (2012).
[37] M. A. Miller and D. Frenkel, Competition of Percolation and Phase Separation in a Fluid of Adhesive Hard Spheres, Phys. Rev. Lett. **90**, 135702 (2003).
[38] M. E. Cates and J. Tailleur, Motility-induced phase separation, Annu. Rev. Condens. Matter Phys. **6**, 219 (2015).
[39] J.-P. Hansen and I. R. McDonald, *Theory of Simple Liquids* (Elsevier, Amsterdam, 1990).
[40] N. de Macedo Biniossek, H. Löwen, Th Voigtmann, and F. Smallenburg, Static structure of active Brownian hard disks, J. Phys.: Condens. Matter **30**, 074001 (2018).
[41] T. Sentjabrskaja, E. Zaccarelli, C. De Michele, F. Sciortino, P. Tartaglia, T. Voigtmann, S. U. Egelhaaf, and M. Laurati, Anomalous dynamics of intruders in a crowded environment of mobile obstacles, Nat. Commun. **7**, 11133 (2016).